

1 **Quantitatively predicting optimal antibiotic dose levels from drug-target binding**

2

3 *Fabrizio Clarelli¹, Adam Palmer², Bhupender Singh¹, Merete Storflor¹, Silje Lauksund¹, Ted*
4 *Cohen³, Sören Abel^{1,4,#}, Pia Abel zur Wiesch^{1,3,#,*}* [ORCID: [https://orcid.org/0000-0001-9420-](https://orcid.org/0000-0001-9420-9005)
5 *9005*]

6

7 1. Department of Pharmacy, Faculty of Health Sciences, University of Tromsø, Tromsø,
8 Norway.

9 2. Laboratory of Systems Pharmacology, Harvard Medical School, Boston, MA, USA.

10 3. Department of Epidemiology of Microbial Diseases, Yale School of Public Health, New
11 Haven, Connecticut, United States of America.

12 4. Centre for Molecular Medicine Norway, Nordic EMBL Partnership, Oslo, Norway.

13 # Authors contributed equally

14 * e-mail: pia.z.wiesch@uit.no

15 **Abstract**

16 Improved predictions of antibiotic efficacy can inform the development of new antibiotics and
17 extend the effectiveness of existing drugs and thereby help combatting the global antibiotic
18 resistance crisis. We describe a computational model (COMBAT- COmputational Model of
19 Bacterial Antibiotic Target-binding) that leverages accessible biochemical parameters to
20 quantitatively predict the antimicrobial effects of antibiotics based on their drug-target affinity.
21 We validate our model with MICs of a range of quinolone antibiotics in clinical isolates
22 demonstrating that antibiotic efficacy can be predicted from drug-target binding ($R^2 > 0.9$).
23 Conversely, we experimentally demonstrate that changes in drug-target binding can be predicted
24 from antibiotic efficacy with 92-94% accuracy by exposing bacteria overexpressing target
25 molecules to ciprofloxacin. To test the generality of COMBAT, we predict target molecule
26 occupancy at MIC from antimicrobial action with 90% accuracy for a different antibiotic class,
27 the beta-lactam ampicillin. Finally, we predict antibiotic concentrations that can select for
28 resistance due to novel resistance mutations. COMBAT provides a framework to inform optimal
29 antibiotic dose levels that maximize efficacy and minimize the rise of resistant mutants.

30

31 **Introduction**

32 The rise of antibiotic resistance represents an urgent public health threat. In order to effectively
33 combat the spread of antibiotic resistance, we must optimize the use of existing drugs and
34 develop new drugs that are effective against drug-resistant strains. Accordingly, methods to
35 improve antibiotic dose levels to i) maximize efficacy against susceptible strains and ii)
36 minimize resistance evolution play a key role in our defense against antibiotic resistant
37 pathogens.

38

39 It is noteworthy that dosing strategies for treatment of susceptible strains (e.g., dosing level¹,
40 dosing frequency², and treatment duration³⁻⁵) have recently been substantially improved, even for
41 antibiotic treatments that have been standard of care for decades. This suggests that there likely
42 remains significant room for optimization in our antibiotic treatment regimens. It also highlights
43 the difficulty in identifying optimal dosing levels for new antibiotics. Indeed, optimizing dosing
44 is one of the biggest challenges in drug development. Typically, time-consuming trial-and-error
45 approaches are used and each failed drug candidate makes this process more expensive⁶.

46

47 It is even more challenging to optimize dose levels to minimize the emergence of antibiotic
48 resistance, both for existing and novel antibiotics. There remains substantial debate about which
49 dosing strategies best prevent the emergence of resistant mutants during treatment⁷⁻⁹. In this
50 context, a useful concept that links antibiotic concentrations with resistance evolution is the
51 resistance selection window (mutant selection window) that ranges from the lowest
52 concentration at which the resistant strain grows faster than the wild-type, usually well below the
53 wild-type minimum inhibitory concentration (MIC), to the MIC of the resistant strain¹⁰⁻¹².

54 Antibiotic concentrations above the resistance selection window safeguard against *de novo*
55 resistance emergence. Antibiotic concentrations below the resistance selection window do not
56 kill the susceptible strain, but also do not favor the resistant strain and therefore do not promote
57 emergence of resistance. The latter may be preferable if one cannot dose above the MIC of the
58 resistant strain due to toxicity or solubility limits. To limit resistance emergence, it is therefore
59 important to identify the resistance selection window and optimize dosing accordingly.

60

61 Limitations in our knowledge of how antibiotic treatment regimens affect bacterial populations
62 contribute to the need for lengthy and expensive trial-and-error approaches, with the sheer
63 number of possible dosing regimens making it difficult to identify an optimal regimen. We argue
64 that this knowledge gap is a major limitation for the improvement of dosing regimens of existing
65 drugs and a real obstacle for the development of new antibiotics^{13,14}.

66

67 Pharmacodynamic models that can make predictions of bacterial killing and selection on the
68 basis of drug-target interactions offer new promise to inform rational antibiotic dosing
69 practices¹⁵. Recently described models that include drug-target binding have been useful in
70 gaining a better qualitative understanding of complicated drug effects, such as post-antibiotic
71 effects, inoculum effects, and bacterial persistence¹⁵⁻¹⁸. However, to speed the development of
72 new antibiotics or to inform practices which minimize resistance, we require quantitative
73 predictions for antibiotics or resistant bacterial strains that do not exist yet. Models which permit
74 quantitative predictions of changes in drug efficacy as a function of modification of antibiotic
75 molecules (i.e. new drugs) or novel resistance mutations would be invaluable. Such tools would
76 advance our general mechanistic understanding of antibiotic action, could guide dosing trials of
77 new drugs, and suggest better dosing of existing drugs.

78

79 In this report, we describe a mechanistic computational modeling framework (COMBAT-
80 COmputational Model of Bacterial Antibiotic Target-binding) that allows us to predict drug
81 effects based solely on accessible biochemical parameters describing drug-target interaction.
82 These parameters can be determined early in drug development. We use this framework to
83 investigate how changes in drug target binding, either due to improvements in existing

84 antibiotics or due to resistance mutations in bacteria, affect antibiotic efficacy. We first show that
85 COMBAT accurately predicts bacterial susceptibility as a function of drug-target binding and,
86 conversely, allows inference of these biochemical parameters on the basis of observed patterns of
87 bacterial growth suppression or killing. We then use COMBAT to predict the susceptibility of
88 newly arising resistant variants based on the molecular mechanism of resistance and determine
89 the resistance selection window.

90

91 **Results**

92 **Quinolone target affinities correlate with antibiotic efficacy**

93 To investigate how biochemical changes in antibiotic action modifies bacterial susceptibility, we
94 explored how the affinity of antibiotics to their target affects the MIC. We compared the MICs of
95 quinolones, an antibiotic class in which individual antibiotics have a wide range of affinities to
96 their target, gyrase ($K_D \sim 10^{-4} - 10^{-7}$ M) but are of similar molecular sizes and have a similar mode
97 of action¹⁹. This choice allowed us to isolate the effects of differences in drug-target affinity on
98 the MIC.

99

100 We obtained binding affinities of quinolones to their gyrase target in *Escherichia coli* from
101 previous studies²⁰⁻²⁴. We then retrieved MIC data for several quinolones from clinical
102 Enterobacteriaceae isolates collected before 1990²⁵, i.e., before the widespread emergence of
103 quinolone resistance¹⁹. We assume that quinolone affinities obtained from clinical
104 Enterobacteriaceae isolates collected before the emergence of resistance correspond to those
105 measured in wild-type *E. coli*.

106

107 To make qualitative predictions of MICs, we employed a simplified model based on the
108 assumptions that i) drug-target binding occurs much more quickly than bacterial replication, ii)
109 the antibiotic concentration remains constant and iii) that during the 18 hours of an MIC assay,
110 the concentration gradient of the drug inside and outside the cell has equilibrated. Under these
111 assumptions, the MIC can be expressed as

$$112 \quad MIC = K_D \frac{f_c}{1-f_c} \quad (1)$$

113
114 where K_D represents the affinity constant and f_c the fraction of the target bound at the MIC²⁶.

115 Accordingly, this model predicts that the MIC is linearly correlated with K_D .

116
117 Fig. 1 shows the correlations between drug-target affinities and MICs for seven quinolones and
118 clinical isolates of 11 different Enterobacteriaceae species. We observed a significant ($p < 0.018$)
119 linear correlation between MIC and K_D in all species, confirming the qualitative model
120 prediction.

121

122 **A quantitative model to predict antibiotic efficacy**

123 While it was encouraging that our model can qualitatively predict MIC changes, our aim was to
124 quantitatively predict antibiotic treatment performance. The simplified model assumes that the
125 binding kinetics are much faster than bacterial replication, which may not be true in all cases. To
126 expand the generalizability of the model, we extended the modeling framework to allow that
127 bacterial replication may occur in a similar time frame as drug-target binding events.

128

129 The full model (COMBAT- COmputational Model of Bacterial Antibiotic Target-binding)
130 describes the binding and unbinding of antibiotics to their targets and predicts how such binding
131 dynamics affects bacterial replication and death (Fig. 2a). In previous work linking drug-target
132 binding kinetics with bacterial replication¹⁸, we described a population of bacteria with θ target
133 molecules per cell with a system of $\theta + 1$ (bacteria with 0, 1, ..., θ bound target molecules)
134 ordinary differential equations (ODEs). This system increases in complexity with the number of
135 target molecules and makes fitting the model to data computationally too demanding for most
136 settings. To simplify this prior approach, we developed new mathematical models based on
137 partial differential equations (PDEs), where a single equation describes all bacteria
138 simultaneously. The sum of bacteria within all target occupancy states over time can be
139 described by a time kill curve (Fig. 2b), during which the bacterial population is characterized by
140 the distribution of bacterial cells with different levels of target occupancies at each time-step
141 (Fig. 2c). This curve can be visualized as a two-dimensional surface in a three-dimensional
142 coordinate system where the number of bacteria is represented on the z-axis, the percent of
143 bacteria with the fraction of bound target molecules on the x-axis, and time on the y-axis (Fig.
144 2d).

145

146 Antibiotic action is described by rates of binding (k_f) and unbinding (k_r) to bacterial target
147 molecules (Fig. 2a, e). The binding of an antibiotic to a target results in the formation of an
148 antibiotic-target molecule complex x , where x ranges between 0 and θ .

149 COMBAT consists of two mass balance equations: equation 2 describing bacterial numbers as a
150 function of bound targets and time and equation 3 describing antibiotic concentration as a
151 function of time (Methods section).

$$152 \quad \frac{\partial B(x,t)}{\partial t} + \overbrace{\frac{\partial}{\partial x} (v_B(x,t)B(x,t))}^{\text{Binding kinetics}} = \overbrace{-r(x)B(x,t)F_{lim}(t) + S_B(x,t)F_{lim}(t)}^{\text{Replication and its effects on binding}} - \overbrace{\delta(x)\vec{B}(x,t)}^{\text{Death}} \quad (2)$$

153

154 The term for binding kinetics is given in brown, the term for replication in blue and the term for
 155 death in red.

$$156 \quad \frac{dA(t)}{dt} = -\hat{k}_f A(t) \int_0^\theta (\theta - x) B(x,t) dx + k_r \int_0^\theta x B(x,t) dx \quad (3)$$

157

158 where $v_B = v_f - v_r$, $v_f = \hat{k}_f A(t)(\theta - x)$ and $v_r = k_r x$. v_B , v_f , and v_r can be seen as a

159 generalized velocity $v = \frac{dx}{dt}$.

160

161 Equation 4 (part of the replication term in equation 2) describes how daughter cells inherit bound
 162 target molecules from the mother cell during replication:

$$163 \quad S_B(x,t) = 2 \int_x^\theta h(x,z)r(z)B(z,t)dz; \forall x \in [0,\theta] \quad (4)$$

164

165 Equation 5 (part of the replication term in equation 2) is a logistic growth model describing
 166 reduced bacterial replication as the carrying capacity is approached:

$$167 \quad F_{lim} = \left(1 - \frac{\int_0^\theta B(x,t)dx}{K} \right) \quad (5)$$

168

169 **Model fit to ciprofloxacin time-kill data**

170 We used the quinolone ciprofloxacin to quantitatively fit bacterial time-kill curves, since this is a
 171 commonly used antibiotic for which binding parameters have been directly measured.

172 Supplementary Tab. S1 gives an overview of the known parameters used for fitting;

173 Supplementary Tab. S2 gives the parameters resulting from our fit.

174

175 The functional relationship between the levels of bacterial replication and death on the fraction
176 of bound target molecules is extremely hard to obtain experimentally. We therefore treated the
177 relationships between the fraction of bound target and bacterial replication and death as free
178 parameters in our model fitting. Ciprofloxacin is considered to have both bacteriostatic and
179 bactericidal action (mixed action)^{27,28}, and we fitted functions for a monotonically decreasing
180 replication and a monotonically increasing killing with each successively bound target molecule
181 (see Methods & Supplementary Fig. S1).

182

183 Overall, we found that COMBAT could fit the time-kill curves well ($R^2 = 0.93$, Fig. 3a). Fig. 3b
184 shows the predicted bacterial replication $r(x)$ and death as a function of target occupancy $\delta(x)$
185 based on the fit obtained in Fig. 3a. After model calibration, we simulated bacterial replication
186 during exposure to different antibiotic concentrations for 18 h. For this simulation, positive
187 values indicate an increase in the number of bacteria, and negative values indicate a decrease in
188 the number of bacteria. We estimated a MIC of 0.0139 mg/L (Fig. 3c), a value that is within the
189 range of MIC determinations for wt *E. coli* (0.01 mg/L, 0.015 mg/L, 0.017 mg/L and 0.023 mg/L
190 ^{11,29-31}).

191 **Accurate prediction of target overexpression from time-kill data**

192 Having shown that COMBAT can quantitatively fit experimental data on antibiotic action within
193 biologically plausible parameters, we continued to test the predictive ability of the model. Given
194 our hypothesis that modifications in antibiotic-target interactions lead to predictable changes in

195 bacterial susceptibility, we experimentally induced changes in the antibiotic-target interaction of
196 ciprofloxacin in *E. coli*. We then quantified these biochemical changes by fitting COMBAT to
197 corresponding time-kill curves and compared them to the experimental results. Ciprofloxacin
198 acts on gyrase A₂B₂ tetramers¹⁹. We used an *E. coli* strain for which both gyrase A and gyrase B
199 are under the control of a single inducible promoter (*P_{lacZ}*), such that the amount of gyrase A₂B₂
200 tetramer can be experimentally manipulated³². We measured net growth rates for this strain at
201 different ciprofloxacin concentrations in the presence of 10 μM isopropyl β-D-1-
202 thiogalactopyranoside (IPTG; mild overexpression) and 100 μM IPTG (strong overexpression)
203 and compared it to the wild-type in the absence of the inducer (Fig. 4a).

204

205 Like previously reported, we find that increasing gyrase content makes *E. coli* more susceptible
206 to ciprofloxacin³². We fitted net growth rates allowing the target molecule content, i.e. gyrase
207 A₂B₂, to vary. We assumed that the only change between the different conditions was the amount
208 of target. We further assumed that the relationship between bound target and bacterial replication
209 or death did not differ between the control strain containing a mock plasmid (no IPTG) and the
210 experiments with overexpression (Fig. 4b, between 0 % and 100 %). Finally, we assumed that
211 the maximal kill rate at very high antibiotic concentrations was accurately measured in our
212 experiments and forced the function describing bacterial death through the measured value when
213 all target molecules are bound. We found the best fit for a 1.31x increase in GyrA₂B₂ target
214 molecule content for bacteria grown in the presence of 10 μM IPTG and a 2.02x increase in
215 GyrA₂B₂ target molecule content for those grown in the presence of 100 μM IPTG.

216

217 We subsequently tested these predictions experimentally by analyzing Gyrase A and B content
218 by western blot Fig. 4c; Supplementary Fig. S2). Using realistic association and dissociation
219 rates for biological complexes³³, we predicted a range of functional tetramers based on the
220 relative amount of Gyrase A and B proteins (Fig. 4d). Supplementary Tab. S3 details the
221 individual measurements, and the procedure to estimate tetramers is provided in the methods
222 section. We found that the observed overexpression was very close to our theoretical prediction,
223 with 1.43x [95 % CI 1.19-1.81] overexpression (model prediction = 1.31x overexpression) in the
224 presence of 10 μ M IPTG and 2.15x [95 % CI 1.73-2.87] overexpression in the presence of
225 100 μ M IPTG (model prediction = 2.02x overexpression).

226

227 **Accurate prediction of target occupancy at MIC from time-kill data**

228 Next, we tested whether COMBAT can be applied to the action of the beta-lactam ampicillin, a
229 very different antibiotic with a distinct mode of action from quinolones. Using published
230 pharmacodynamic data of *E. coli* exposed to ampicillin³¹ also allowed us to compare COMBAT
231 predictions to established pharmacodynamic approaches. Most of the biochemical parameters for
232 ampicillin binding to its target, penicillin-binding proteins (PBPs), have been determined
233 experimentally (Supplementary Tab. S1). Ampicillin is believed to act as a bactericidal drug³⁴,
234 and this mode of action is supported by findings from single-cell microscopy²⁶. We therefore
235 assume that ampicillin binding does not affect bacterial replication. In order to model the
236 consumption of beta-lactams at target inhibition and eventual target recovery, we made small
237 adjustments to equation 13 (see Methods, description of beta-lactam action).

238

239 We fitted COMBAT to published time-kill curves of *E. coli* exposed to ampicillin (Fig. 5a).
240 Again, COMBAT provides a good fit to the experimental data between 0 min and 40-60 min.
241 After that time, observed bacterial killing showed a characteristic slowdown at high ampicillin
242 concentrations which is often attributed to persistence¹⁸ (Fig. 5a). For the sake of simplicity, we
243 chose to omit bacterial population heterogeneity in this work and therefore cannot describe
244 persistence, even though COMBAT can be adapted to capture this phenomenon¹⁸. Because
245 ampicillin acts in an entirely bactericidal manner, we assume a constant replication rate (see
246 Methods & Supplementary Fig. S1) and fitted bacterial death as a function of target binding,
247 $\delta(x)$ (Fig. 5b, fitted parameters in Tab. S4). Fig. 5c shows the predicted net growth rate over a
248 range of drug concentrations. We estimated a MIC of 2.6 mg/L. This MIC is based on the
249 Clinical & Laboratory Standards Institute definition of the MIC determined at 18 h. The original
250 source of the MIC, which was based on experimental data and a pharmacodynamic model³¹
251 determined an MIC of 3.4 mg/L at 1 h. If we change our prediction to 1 h, our estimated MIC is
252 3.32 mg/L, which is within 2.5 % of the reported value³¹.

253

254 Having established that COMBAT can also adequately capture the pharmacodynamics of
255 ampicillin, we next tested whether we can estimate experimentally determined target occupancy
256 at the MIC. Our estimated mean occupancy considering both living and dead bacteria is 89 %
257 (Fig. 5b), a value within previously reported experimental estimates from *Staphylococcus aureus*
258 (84-99 %) ³⁵.

259

260 **Sensitivity of antibiotic efficacy to parameters of drug-target binding**

261 It is possible to vary all parameters in COMBAT and explore their effect. We used this to test
262 how hypothetical chemical changes to ampicillin or ciprofloxacin would affect antibiotic
263 efficacy (Supplementary Fig. S3-S11). These changes could reflect either bacterial resistance
264 mutations or modifications of the antibiotics themselves. We predict that changes in drug-target
265 affinity, K_D , have more profound effects than changes in target molecule content, bacterial
266 reaction to increasingly bound target (i.e. $\delta(x)$ and $r(x)$), or changes in target molecule content.
267 We also predict that the individual binding rates k_r and k_f , and not just the ratio of these terms,
268 the K_D , are important factors in efficiency. The faster a drug binds, the more efficient we
269 predicted it will be. One intuitive explanation for the observation that k_f drives efficacy is that a
270 slow binding fails to rapidly interfere with bacterial replication, which may allow for the
271 production of additional target molecules and thereby reduce the ratio of free antibiotic to target
272 molecules.

273

274 **Forecasting the resistance selection window**

275 Finally, we illustrate how COMBAT can be used to explore how the molecular mechanisms of
276 resistance mutations affect antibiotic concentrations at which resistance can emerge, i.e., the
277 resistance selection window. We compared predicted net growth rates as a function of
278 ciprofloxacin concentrations for a wild-type strain and an archetypal resistant strain. For this
279 analysis, we assumed that the resistant strain has a 100x slower drug-target binding rate (i.e.
280 ~100x increased MIC, realistic for novel point mutations³⁶) and that the maximum replication
281 rate of the resistant strain is 85 % of the wild type strain³⁷. We then predicted the antibiotic
282 concentrations at which resistance would be selected. Interestingly, when comparing COMBAT
283 to previous pharmacodynamics models (Fig. 5), we observed that estimates of replication rates

284 depend on the selected time frame (Fig. 6a). When the timeframe for MIC determination is set to
285 18 h as defined by CLSI³⁸, the “competitive resistance selection window”, i.e., the concentration
286 range below the MIC of both strains where the resistant strain is fitter than the wild type, ranges
287 from 0.002 mg/L to 0.014 mg/L for ciprofloxacin (Fig. 6a) and 1 mg/L to 2.6 mg/L for
288 ampicillin (Supplementary Fig. S12), respectively. This corresponds well with previous
289 observations that ciprofloxacin resistance is selected for well below MIC¹¹. However, when
290 measuring after 15 min or 45 min, the results are substantially different. The reason for this is
291 illustrated in Fig. 6b. COMBAT reproduces non-linear time kill curves where bacterial
292 replication continues until sufficient target is bound to result in a negative net growth rate. This
293 compares well with experimental data around MIC in Fig. 3a and 5a. In Fig. 6b, we show model
294 predictions for ciprofloxacin concentrations corresponding to a zero net growth (i.e. same
295 population size) after 15 min, 45 min and 18 h ($MIC_{Resistant; 15 \text{ min}}$, $MIC_{Resistant; 45 \text{ min}}$,
296 $MIC_{Resistant; 18 \text{ h}}$). In all cases, the bacterial population first increases and then decreases slowly.
297 This may have consequences for the selection of resistant strains. Fig. 6c illustrates how the
298 resistance selection windows depending on the observed time frame. This suggests that even at
299 concentrations above the 18 h MIC of the resistant strain, there may be initial growth of the
300 resistant strain. In this case, the resistant strain could continue growing at concentration of up to
301 7 mg/L ciprofloxacin at 15 min, even though the MIC at 18 h is 1.27 mg/L.

302

303 **Discussion**

304 Optimizing dosing levels of antibiotics is important for maximizing drug efficacy against wild-
305 type strains as well as for minimizing the rise of resistant mutants. The determination of optimal
306 dosing strategies typically requires expensive empirical studies; the need for such studies arises
307 in part from our currently limited capacity to predict how antibiotics will affect bacteria at a

308 given concentration. In fact, drug attrition is mainly due to insufficient predictions of efficacy
309 (pharmacodynamics) rather than pharmacokinetics⁶. For optimizing drug development and for
310 minimizing resistance, we need quantitative predictions for antibiotics or resistant bacterial
311 strains that do not exist yet. The ability to accurately predict MICs on the basis of biochemical
312 parameters and, more generally, to define antibacterial activity across a range of drug
313 concentrations, would allow us to estimate antibiotic efficacy for novel compounds or against not
314 yet emerged resistant strains^{15,39}. Recent studies have reported methods to predict MICs from
315 whole genome sequencing data^{40,41}. However, these methods require transfer of prior knowledge
316 on how the resistance mutations affect MICs in other organisms. There are no methods that could
317 predict *a priori* how chemical changes to an antibiotic structure or novel resistance mutations
318 affect bacterial growth at a given antibiotic concentration.

319
320 Here, we accurately predict antibiotic action on the basis of accessible biochemical parameters of
321 drug-target interaction. Our computational model, COMBAT provides a framework to predict
322 the efficacy of compounds based on drug-target affinity, target number, and target occupancy.
323 These parameters may change both when improving antibiotic lead structures as well as when
324 bacteria evolve resistance. Importantly, they can be measured early in drug development and
325 may even be a by-product of target-based drug discovery⁴². When these data are available,
326 COMBAT makes only one assumption: that the rate of bacterial replication decreases and/or the
327 rate of killing increases with successive target binding. While fitting, we allow this relationship
328 to be gradual or abrupt and select the best fit. This means we do not model specific molecular
329 mechanisms down-stream of drug-target binding, but their effects are subsumed in the functions
330 that connect the kinetic of drug-target binding to bacterial replication and death.

331
332 In previous work, for example on antipsychotics¹⁶, antivirals¹⁷ and antibiotics^{15,18}, models of
333 drug-target binding kinetics have been used to improve our qualitative understanding of
334 pharmacodynamics. Our study substantially advances this work by making accurate quantitative
335 predictions across antibiotics and bacterial strains when measurable biochemical characteristics
336 change. This is possible because COMBAT employs an elegant mathematical approach, based
337 on partial differential equations, that makes it computationally feasible to fit the model to a large
338 range of data. Importantly, we are not only able to predict antibiotic action from biochemical
339 parameters, but can also vice versa use COMBAT to accurately predict biochemical changes
340 from observed patterns of antibiotic action. We have confirmed the excellent predictive power of
341 COMBAT with clinical data as well as experiments with antibiotics with very different
342 mechanisms of action. This gives us confidence that biochemical parameters are major
343 determinants of antibiotic action in bacteria and that COMBAT helps to make rational decisions
344 about antibiotic dosing.

345
346 In drug development, our mechanistic modeling approach provides insight into which chemical
347 characteristics of drugs may be useful targets for modification. For example, our sensitivity
348 analyses indicate that antibiotics with a similar affinity but faster binding inactivate bacteria
349 more quickly and therefore prevent replication and production of more target molecules, which
350 would change the ratio of antibiotic to target. Furthermore, because e.g. antibiotic binding and
351 unbinding rates can be determined early in the drug development process, such insight can help
352 the transition to preclinical and clinical dosing trials. This may contribute to reducing bottlenecks
353 between these phases of drug development and thereby save money and time.

354

355 Avoiding antibiotic concentrations that select for resistance is challenging because the precise
356 concentrations are only known after extensive experiments have been performed that identify the
357 MIC of (nearly) all possibly emerging resistant mutants. Predicting the resistance selection
358 windows of novel resistant mutants on the basis of biologically plausible changes in drug-target
359 binding would allow us to better assess what drug concentrations need to be achieved to avoid
360 selection of resistance. This approach offers new promise to assess resistance risks prior to
361 characterizing the majority of resistance mutations and thereby reduce the failure rates of
362 candidate compounds late in the drug development process when resistance is observed in
363 patients and substantial resources have been invested.

364

365 Our approach also offers insight into determinants of the resistance selection window. Rather
366 than determining the resistance selection window for a comprehensive collection of possibly
367 arising resistance mutations in each bacteria-drug pair, it would be attractive to build
368 transferrable knowledge that allows estimating the resistance selection window. In concordance
369 with a recent meta-analysis of experimental data⁴³, our sensitivity analyses predict that changes
370 in drug target binding and unbinding have a greater impact on the MIC than changes in target
371 molecule content or down-stream processes. Thus, a more comprehensive characterization of the
372 binding parameters of spontaneous resistant mutants would allow an overview of the maximal
373 biologically plausible levels of resistance that can arise with one mutation. Dosing above this
374 level should then safeguard against resistance. This is especially useful for compounds for which
375 it is difficult to saturate the mutational target for resistance, or for safeguarding against resistance
376 to newly introduced antibiotics for which we do not yet have a good overview of resistance

377 conferring mutations. If toxicity, solubility or other constraints do not allow dosing above the
378 MIC of expected resistant strains, COMBAT can predict the concentration range at which
379 resistance is less strongly selected. This could guide decisions on treating with low versus high
380 doses, which is currently controversially debated^{7,8}. Good quantitative estimates on the dose-
381 response relationship of new drugs would also help defining the therapeutic window, i.e. the
382 range of drug concentrations at which the drug is effective but not yet toxic.

383

384 Our quantitative work can help to identify optimal dosing strategies at constant antibiotic
385 concentrations for homogeneous bacterial populations. These measures are commonly used to
386 assess antibiotic efficacy. In addition, previous work has demonstrated that drug-target binding
387 models can qualitatively describe antibiotic efficacy over the fluctuating concentrations that
388 actually occur in patients^{26,44}. They can also explain complicated phenomena such as biphasic
389 kill curves, the post-antibiotic effect, or the inoculum effect^{15,18,45} that often complicate the
390 clinical phase of drug development. COMBAT has similar characteristics that allow capturing
391 these complex phenomena. Therefore, employing COMBAT may be useful for guiding drug
392 development to maximize antibiotic efficacy and minimize *de novo* resistance evolution.

393

394 **Methods**

395 ***Mathematical model***

396 COMBAT incorporates the binding and unbinding of antibiotics to their targets and describes
397 how target binding affects bacterial replication and death. This work extends the model
398 developed in¹⁸. COMBAT consists of a system of two mass balance equations: one PDE for

399 bacteria (describing replication and death as a function of both time and target binding) and one
400 ODE for antibiotic molecules (describing the concentrations as function of time).

401

402 In the most basic version of COMBAT, we ignored differences between extracellular and
403 intracellular antibiotic concentrations and only followed the total antibiotic concentration A ,
404 assuming that the time needed for drug molecules to enter bacterial cells is negligible. We model
405 ciprofloxacin (to which there is a limited diffusion barrier⁴⁶) and ampicillin (where the target is
406 not in the cytosol, even though the external membrane in gram negatives has to be crossed to
407 reach PBPs). We therefore believe that this assumption is justified in wild-type *E. coli*. This
408 basic version of COMBAT is therefore more accurate for describing antibiotic action where the
409 diffusion barrier to the target is weak.

410

411 *Binding kinetics*

412 We describe the action of antibiotics as a binding and unbinding process to bacterial target
413 molecules¹⁸. For simplicity, we assume a constant number of available target molecules θ . The
414 binding process is defined by the formula $A + T \rightleftharpoons x$, where the intracellular antibiotic
415 molecules A react with target molecules T at a rate k_f and form an antibiotic-target molecule
416 complex x , where values for x range between 0 and θ . If the reaction is reversible, the complex
417 dissociates with a rate k_r .

418 In¹⁸, the association and dissociation terms are described by the following terms

$$\begin{aligned} 420 \quad \frac{dB_i(t)}{dt} = & \overbrace{\hat{k}_f A(t) ((\theta - i + 1)B_{i-1}(t) - (\theta - i)B_i(t))}^{\text{Association term}} - \\ 419 \quad & \overbrace{k_r (iB_i(t) - (i + 1)B_{i+1}(t))}^{\text{Dissociation term}}; \quad i \in [0, \theta] \end{aligned} \quad (6)$$

421

422 where $\hat{k}_f = \frac{k_f}{V_{tot}n_A}$, k_f is the association rate, V_{tot} is the volume in which the experiment is
423 performed, n_A is Avogadro's number, k_r is the dissociation rate, B_i is the number of bacteria with
424 i bound targets, and θ is the total number of targets. Green denotes the association term, while
425 the dissociation term is in orange.

426 This approach requires the use of a large number of ordinary differential equations, $(\theta + 1)$ for
427 the bacterial population and one for the antibiotic concentration. To generalize this approach, we
428 assume that the variable of bound targets is a real number $x \in \mathcal{R}$. Under this continuity
429 assumption, we consider the bacterial cells as a function of x and the time t , thereby reducing the
430 total number of equations to two.

431 Under the continuity approximation ($x \in \mathcal{R}$), we can rewrite the binding kinetics in the form

$$432 \quad \frac{\partial B(x,t)}{\partial t} = \overbrace{\frac{\partial}{\partial x} \left(\hat{k}_f A(t) (\theta - x) B(x,t) \right)}^{\text{Association term}} - \overbrace{\frac{\partial}{\partial x} \left(k_r x B(x,t) \right)}^{\text{Dissociation term}} \quad (7)$$

433

434 or simply

$$435 \quad \frac{\partial B(x,t)}{\partial t} = \frac{\partial}{\partial x} \left(v_f(x,t) B(x,t) - v_r(x,t) B(x,t) \right) \quad (8)$$

436

437 where $v_f = \hat{k}_f A(t) (\theta - x)$ and $v_r = k_r x$ can be considered as two velocities, i.e., the derivative
438 of the bound targets with respect to the time $\frac{dx}{dt}$. Green denotes the association term, while the
439 dissociation term is in orange.

440

441 *Replication rate*

442 We assume that the replication rate of bacteria, $r(x)$, is dependent on the number of bound target
443 molecules x . The function $r(x)$ is a monotonically decreasing function of x , such that fewer
444 bacteria replicate as more target is bound. $r(0)$ is the maximum replication rate, corresponding to
445 the replication rate of bacteria in absence of antibiotics. Thus, $r(x)$ describes the bacteriostatic
446 action of the antibiotics, i.e., the effect of the antibiotic on bacterial replication.

447

448 *Carrying capacity*

449 Replication ceases as the total bacterial population approaches the carrying capacity K . At that
450 point, the replication term of the equation is

$$451 \frac{\partial B(x,t)}{\partial t} = r(x)B(x,t) \frac{K - \int_0^\theta B(x,t) dx}{K} = r(x)B(x,t)F_{lim} \quad (9)$$

452

453 where $F_{lim} = \frac{K - \int_0^\theta B(x,t) dx}{K}$ is the replication-limiting term due to the carrying capacity K , and

$$454 0 \leq F_{lim} \leq 1.$$

455

456 *Distribution of target molecules upon division*

457 We assume that the total number of target molecules doubles at replication, such that each
458 daughter cell has the same number as the mother cell. We also assume that the total number of
459 drug-target complexes is preserved in the replication and that the distribution of x bound target
460 molecules of the mother cell to its progeny is described by a hypergeometric sampling of n
461 molecules from x bound and $2\theta - x$ unbound molecules. Under the continuity assumption, we
462 generalize the concept of hypergeometric distribution. Because the hypergeometric distribution
463 is a function of combinations and because a combination is defined as function of factorials, we

464 can use Γ functions in place of factorials and redefine a continuous hypergeometric distribution
465 as a function of Γ functions. A Γ function is

$$466 \quad \Gamma(\zeta) = \int_0^{\infty} x^{\zeta-1} e^{-x} dx; \operatorname{Re}(\zeta) > 0 \quad (10)$$

467

468 where ζ is a complex number. In this way, the distribution can be expressed as a probability
469 density function of continuous variables. The amount of newborn bacteria is given by the term
470 $r(x)B(x, t)F_{lim}(t)$. We assume that bound target molecules are distributed randomly between
471 mother and daughter cells, with each of them inheriting 50% upon division on average. This
472 means that twice the amount of newborn cells must be redistributed along x to account for the
473 random distribution process. For example, if a mother cell with 4 bound targets divides, we have
474 two daughter cells, each with a number of bound targets between 0 and 4 (their sum has to be 4),
475 following the generalized hypergeometric distribution. For simplicity, we define $S(x, t)$ to be a
476 function related to the replication rate that depends on the number of bacteria with a number of
477 bound target molecules ranging between x and θ , their specific replication rate $r(x)$, and the
478 fraction of their daughter cells expected to inherit x antibiotic-target complexes $h(x, z)$:

$$479 \quad S(x, t) = 2 \int_x^{\theta} h(x, z)r(z)B(z, t) dz \quad (11)$$

480

481 *Death rate*

482 The death rate function $\delta(x)$ depends on the number of bound target molecules. The function
483 $\delta(x)$ is assumed to be a monotonically increasing function of x , where $\delta(\theta)$ is the maximum
484 death rate, when all targets in the bacteria have been bound by antibiotics. The shape of this
485 function describes the bactericidal action of the antibiotic.

486

487 *Bacteriostatic and bactericidal effects*

488 We consider several potential functional forms of the relationship between the percentage of
489 bound targets and replication and death rates, because the exact mechanisms how target
490 occupancy affects bacteria is unknown (Supplementary Fig. S1). We use a sigmoidal function
491 that can cover cases ranging from a linear relationship to a step function. When the inflection
492 point of a sigmoidal function is at 0 % or 100 % target occupancy, the relationship can also be
493 described by an exponential function. We assume that replication in bactericidal and death in
494 bacteriostatic drugs is independent of the amount of bound target. With sufficient experimental
495 data, the replication rate $r(x)$ and/or the death rate $\delta(x)$ can be obtained by fitting COMBAT to
496 time-kill curves of bacterial populations after antibiotic exposure. The sigmoidal shape of $r(x)$
497 and $\delta(x)$ can be written as:

498
$$r(x) = \frac{r_0}{1+e^{\gamma_r(x-x_{rth})}}; \delta(x) = \frac{d_{max}}{1+e^{-\gamma_d(x-x_{dth})}} \quad (12)$$

499

500 where x_{rth} is the replication rate threshold, x_{dth} is the death rate threshold, and both represent the
501 point where the sigmoidal function reaches $\frac{1}{2}$ of its maximum. γ_r and γ_d represent the shape
502 parameters of the replication and death rate functions, respectively. These factors determine the
503 steepness around the inflection point. When they are extreme, the relationship approaches a
504 linear or a step function.

505

506 *Full equation describing bacterial population*

507 Putting these components together, the full equation describing a bacterial population is:

$$\begin{aligned} 508 \quad & \frac{\partial B(x,t)}{\partial t} + \overbrace{\frac{\partial}{\partial x} \left(v_f(x,t)B(x,t) - v_r(x,t)B(x,t) \right)}^{\text{Binding kinetics}} = \\ 509 \quad & \underbrace{-r(x)B(x,t)F_{lim}(t) + S_B(x,t)F_{lim}(t)}_{\text{Replication and its effects on binding}} - \underbrace{\delta(x)B(x,t)}_{\text{Death}} \end{aligned} \quad (13)$$

510

511 where $B(x,t)$ is the number of bacteria. As in equations 2, 6, 7 and 8, green denotes the binding
512 term, orange the unbinding term (together the binding kinetics is given in brown), blue the term
513 describing bacterial replication and red the term describing bacterial death.

514

515 *Equation describing antibiotic concentration*

516 The free antibiotic concentration results from mass conservation, i.e., all antibiotic molecules
517 associating with their target are subtracted and all dissociating antibiotic molecules are added.
518 Equation 3 in the results section describes the dynamics of the antibiotic concentration.

519

520 *Description of beta-lactam action*

521 Beta-lactams acetylate their target molecules (PBPs) and thereby inhibit cell wall synthesis. The
522 acetylation of PBPs consumes beta-lactams. However, PBPs can recover through deacetylation.
523 We modified the term of drug-target dissociation in the equation describing antibiotic
524 concentrations (equation 3), and set the unbinding rate $k_r = 0$. To reflect the recovery of target
525 molecules, we substituted the dissociation rate k_r in the equation describing the bacterial
526 population with the deacetylation rate k_a , as described in²⁶.

527

528 *Initial and boundary conditions*

529 At $t = 0$, we assume that all bacteria have zero bound targets ($x = 0$), and the initial
530 concentration of bacteria is $B(x, 0) = 0, x > 0$, and $B(0,0) = B_0$.

531 At the boundaries of the partial differential equation ($x = 0, x = \theta$), we specify that the outgoing
532 velocities are zero. For $x = 0$, i.e. no bound target molecules, the unbinding velocity $v_r(0, t) =$
533 0 , and in $x = \theta$, i.e. all targets are bound, the binding velocity $v_f(\theta, t) = 0$. When the
534 replication term at $x = 0$ and the death term at $x = \theta$ are known, we can solve the partial
535 differential equation with two ordinary differential equations at the boundaries. They are similar
536 to the equations at $x = 0$ and at $x = \theta$ described by Abel zur Wiesch et al.¹⁸, but taking into
537 account that x is a continuous variable instead of a natural number.

538

539 *Numerical schemes*

540 To solve our system of differential equations, we used a first-order upwind scheme. Specifically,
541 we used the spatial approximation $u_-^f = \frac{u^{(i)} - u^{(i-1)}}{\Delta x}$ for the binding term ($v_f > 0$) and the spatial
542 approximation $u_+^f = \frac{u^{(i+1)} - u^{(i)}}{\Delta x}$ for the unbinding term ($v_r < 0$). For the time approximation of
543 both the PDEs and the ODEs, we used the forward approximation $\frac{\Delta B}{\Delta t} = \frac{B^{n+1} - B^n}{\Delta t}$ ⁴⁷. We also
544 verified that the Courant-Friedrichs-Lewy condition is satisfied. For fitting the experimental data
545 of bacteria exposed to ciprofloxacin and ampicillin, we used the particle swarm method
546 (“particleswarm” function in Matlab, MathWorks software).

547

548 *Concentrations of gyrase A_2B_2 tetramers*

549 We assumed that gyrases A and B first homo-dimerize to A_2 and B_2 , respectively, which in turn
550 bind to each other to form the tetramer TR ⁴⁸. The following system of equations describes their
551 binding kinetics:

$$552 \begin{cases} \frac{dA}{dt} = -2k_1A^2 + 2k_{-1}A_2 \\ \frac{dB}{dt} = -2k_2B^2 + 2k_{-2}B_2 \\ \frac{dA_2}{dx} = k_1A^2 - k_{-1}A_2 - k_3A_2B_2 + k_{-3}TR \\ \frac{dB_2}{dt} = k_2B^2 - k_{-2}B_2 - k_3A_2B_2 + k_{-3}TR \\ \frac{dTR}{dt} = k_3A_2B_2 - k_{-3}TR \end{cases} \quad (14)$$



554

555 First, we calibrated the model to ensure that we obtain the correct number of gyrase A_2B_2
556 tetramers (~ 100) per wild type bacterial cell^{49,50}. This results in an average of each 206 gyrase A
557 and B monomers. Because the association and dissociation rates of the dimers and tetramers are
558 unknown, we sampled 10^4 sets of six parameters in equation 14 (k_{-3}, \dots, k_3) in a Latin hypercube
559 approach from a biologically plausible range where the association rates are between $10^7 - 10^9$
560 $M^{-1} s^{-1}$ and the dissociation rates between $10^{-3} - 10^{-1} s^{-1}$ ³³. This results in 10^4 estimates for each of
561 the six experimental replicates quantifying gyrase A and B (Fig. 4, Supplementary Fig. S2,
562 Supplementary Tab. S3).

563

564 ***Experimental methods***

565 *Strains, growth conditions and strain construction*

566 *Escherichia coli* strain BW25113⁵¹ (SoA2740) was transformed with plasmids pCA24N-SC101-
567 *gyrAB*³² and pCA24N-SC101- Δ P-YFP³² using electroporation, resulting in strains
568 BW25113/pCA24N-SC101-*gyrAB* (SoA3329) and BW25113/pCA24N-SC101- Δ P-YFP
569 (SoA3330), respectively. pCA24N-SC101-*gyrAB* encodes the *E. coli gyrAB* genes under control
570 of the IPTG inducible LacZ promoter. pCA24N-SC101- Δ P-YFP encodes a promoterless copy of
571 YFP and was used as a control. Bacteria were grown at 30°C on either LB agar or in LB broth,
572 both supplemented with 10 μ g/mL chloramphenicol (Cm) and 10 μ M (mild induction) or 100
573 μ M (strong induction) of isopropyl β -D-1-thiogalactopyranoside (IPTG) (43714 5X, VWR
574 Chemicals) when necessary.

575

576 *Time-kill curves*

577 Overnight cultures of BW25113 or SoA3329 and SoA3330 were diluted 1:1000 in pre-warmed
578 LB or LB-Cm and LB-Cm-IPTG, respectively, and grown with shaking to OD₆₀₀ ~0.5. A 1:3
579 dilution series of ciprofloxacin was made and added to the cultures at indicated concentrations.
580 Additional cultures without antibiotics and with a very high concentration of ciprofloxacin
581 (2.187 mg/L) were used to determine the minimal and maximal kill rate, respectively. Samples
582 were taken immediately prior to addition of the antibiotic and in ~20 min intervals or after 45
583 min, respectively. Samples were washed once in phosphate buffered saline (PBS) before colony
584 forming units (CFUs) were determined for each sample by plating a 1:10 dilution series in PBS
585 on LB agar plates.

586

587 *GyrAB* quantification

588 To quantify the relative amount of GyrAB, samples of SoA3329 and SoA3330 were collected
589 after 45 min of drug treatment as described above. An equal number of cells corresponding to 1
590 mL culture at $OD_{600} = 1$ were harvested by centrifugation. Pelleted cells were lysed at room
591 temperature for 20 min using B-PER bacterial protein extraction reagent (90078, Thermo
592 Scientific) supplemented with 100 $\mu\text{g}/\text{mL}$ lysozyme, 5 units/mL DNaseI (all part of B-PER™
593 with Enzymes Bacterial Protein Extraction Kit, 90078, Thermo Scientific) and 100 $\mu\text{M}/\text{mL}$
594 PMSF (52332, Calbiochem). Samples were stored at -80°C until further use.
595 Samples were heated to 70°C for 10 min after addition of 1x Bolt sample reducing agent (B0009,
596 Life Technologies) and 1x fluorescent compatible sample buffer (LC2570, Invitrogen). Proteins
597 in whole-cell lysates were separated on 4-15 % Mini-Protean TGX Precast gels (456-1085, Bio-
598 Rad) and transferred to 0.2 μm Nitrocellulose membranes (1704158, Bio-Rad).
599 Membranes were blocked in Odyssey blocking buffer-TBS (927-50000, Li-Cor) for at least one
600 hour at room temperature. Primary antibodies raised against GyrA (Rabbit α -Gyrase A, PA005,
601 Inspiralis), GyrB (Rabbit α -Gyrase B, PB005, Inspiralis), and CRP (Mouse α -*E. coli* CRP,
602 664304, Nordic Biosite antibodies) were diluted 1:250, 1:250, and 1:2,000 in Odyssey blocking
603 buffer-TBS, respectively. The blocked membranes were incubated with the appropriate primary
604 antibodies overnight at 4°C , washed 4x for 15 min each in TBS-T solution (Tris buffered saline
605 supplemented with Tween20: 0.138 M sodium chloride, 0.0027 M potassium chloride, 0.1 %
606 Tween20, pH 8.0 at 25°C), and incubated for 2 h at room temperature with fluorescent labelled
607 secondary antibodies (1:10,000 of IRDye® 680RD Goat anti-Mouse IgG, P/N 925-68070, Li-
608 Cor and 1:5000 of IRDye® 800CW Goat anti-Rabbit IgG, P/N 925-32211, Li-Cor) in Odyssey
609 blocking buffer-TBS. Finally, the membranes were washed 4x for 15 min each in TBS-T
610 solution and imaged at 700 nm and 800 nm using a Li-Cor Odyssey Sa scanning system.

611 Band intensities were quantified from unmodified images using the record measurement tool of
612 Photoshop CS6, normalized to the CRP loading control after background subtraction, and
613 reported relative to SoA3330. For clarity, the “levels” tool of Photoshop CS6 was used to
614 enhance the contrast of shown Western blot images.

615

616 **Data Availability**

617 Computer code will be available at <https://www.abel-zur-wiesch-lab.com/>.

618

619 **References**

620

621 **Acknowledgements**

622 We thank Giovanni Montani, Forrest W. Crawford, Roberto Natalini, Klaus Harms, Christoph
623 Zimmer, Angelo Vannozzi, Jingyi Liang, Vi Tran, Antal Martinecz and Rafal Mostowy for
624 helpful discussions and feedback on the manuscript. We would like to acknowledge R. Regoes
625 for providing previously published raw data. This work was funded by Bill and Melinda Gates
626 Foundation Grant OPP1111658 (to T.C. & P.AzW.), Research Council of Norway (NFR) Grant
627 262686 (to P.AzW.) and 249979 (to S.A.), and Helse-Nord Grant 14796 (to S.A.).

628

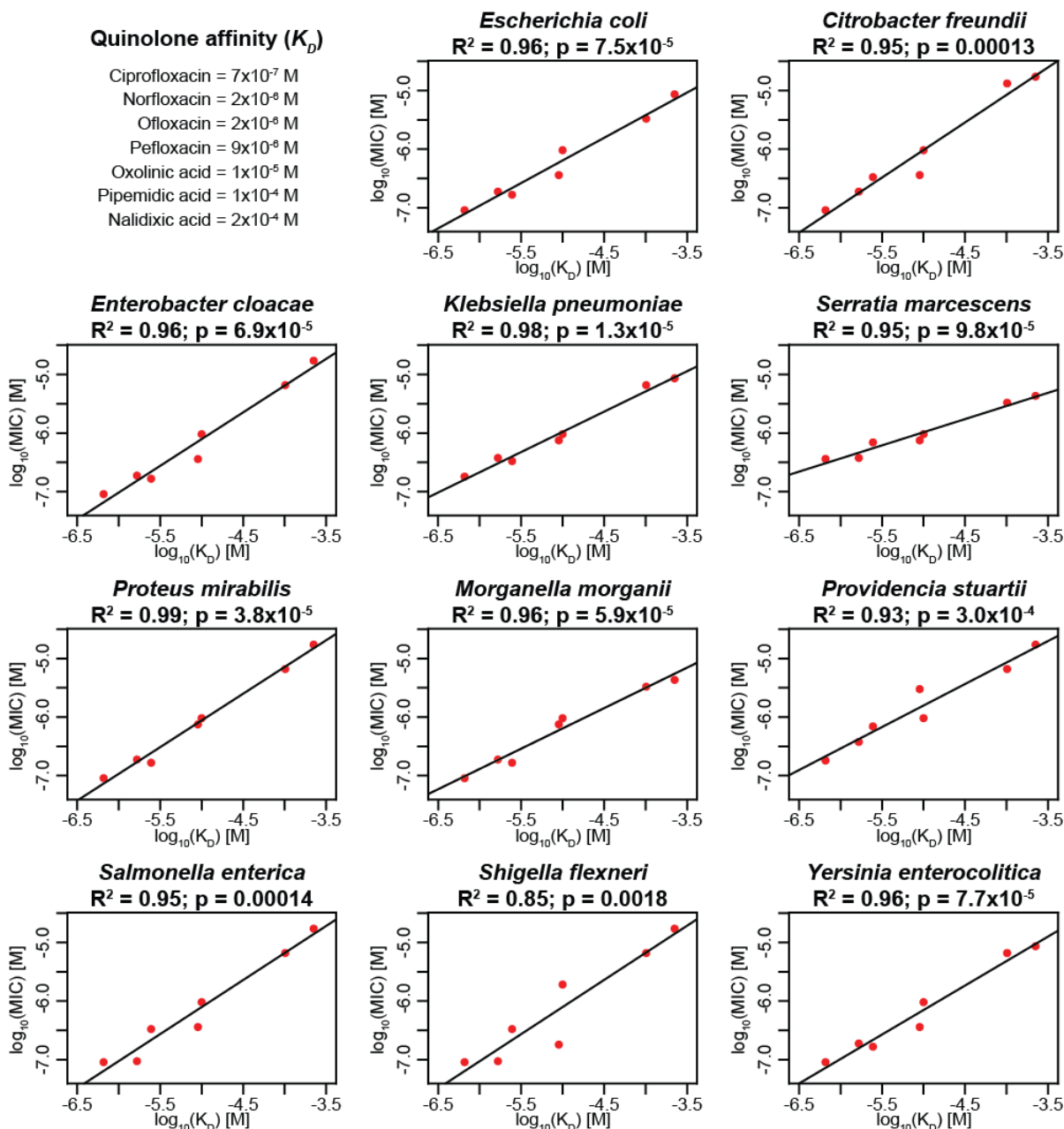
629 **Author Contributions**

630 P.AzW. designed the study. F.C. developed the mathematical models. A.P., B.S., M.S., and S.A.
631 designed the experiments. A.P., B.S., M.S., and S.L. performed the experiments. F.C., A.P., B.S.,
632 M.S., T.C., S.A., and P.AzW. analyzed the data. T.C., S.A., and P.AzW. wrote the manuscript.

633

634 **Competing Interests statement**

635 The authors declare no competing interests.



636

637 **Fig. 1| Clinical data confirm linear correlation between MICs and affinities of quinolones to**

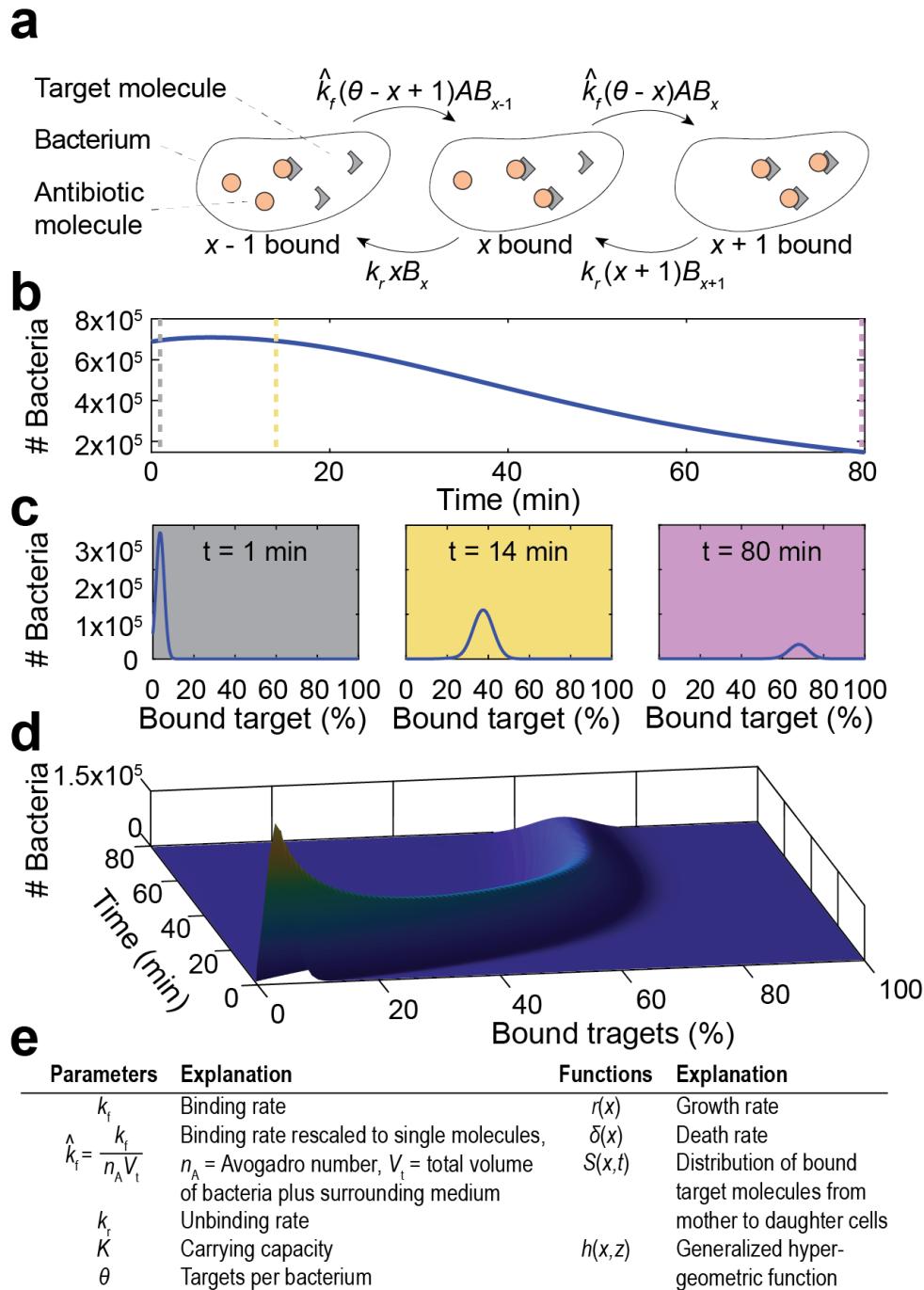
638 **gyrase.** We analyzed MIC and drug-target affinity data from 11 Enterobacteriaceae isolates and

639 seven different quinolones. The x-axes show the affinities (K_D), and the y-axes show the MICs,

640 both in mol/L. The adjusted R^2 and p-value of each correlation are given. In cases where there

641 was more than one K_D value reported in the literature, we used the mean for this analysis. The

642 tested MIC values are the median of several clinical isolates described previously²⁵.



643

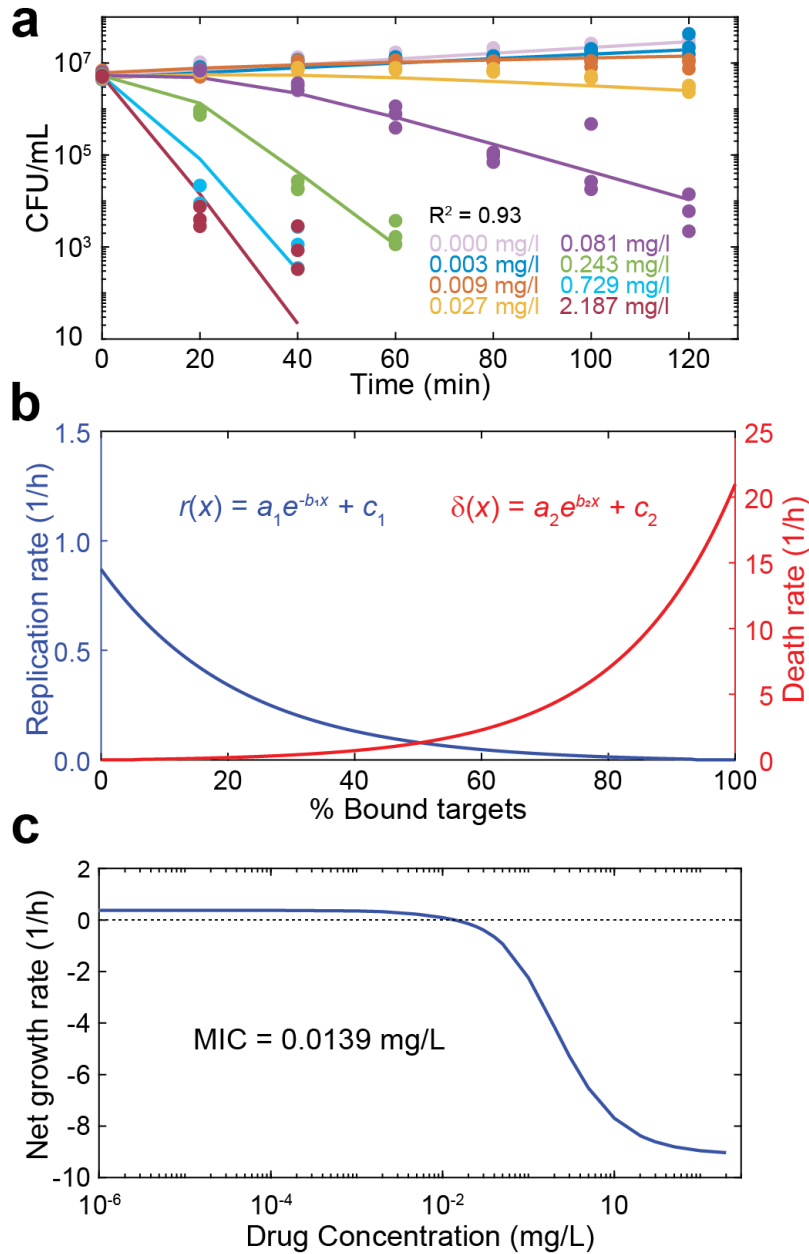
644 **Fig. 2| Illustration of modeling approach. a**, Schematic illustration of binding kinetics (adapted

645 from⁵²). The grey triangles depict the drug target molecules, and the orange circles represent

646 antibiotic molecules within bacteria. The arrows indicate individual binding and unbinding

647 events of the antibiotic to its target molecule in the cell. \hat{k}_f is the adjusted forward reaction rate,

648 k_r is the reverse reaction rate, A is the concentration of antibiotics inside the bacterium, x is the
649 number of bound targets, θ is the number of targets and B_x is the number of bacteria with x bound
650 targets. **b**, Modeled sample time-kill curve, in which the sum of bacteria in all binding states (i.e.,
651 the entire population of living bacteria) is followed over time after exposure to antibiotics. The
652 vertical dotted lines indicate the time points depicted in **(c)**; 1 min (grey), 14 min (yellow), and
653 80 min (purple). **c**, The percentage of bound antibiotic targets in the bacterial population at
654 indicated time points. **d**, Illustration of how the partial differential equation describes the
655 bacterial population as a surface in a three-dimensional coordinate system, the dimensions of
656 which represent percent bound target (x-axis), time (y-axis), and number of bacteria (z-axis). The
657 three time points shown in **(c)** represent two-dimensional cross-sections at different points of the
658 y-axis. **e**, Overview of used parameters and functions.



659

660 **Fig. 3| Model predictions for the MIC and the bacteriostatic and bactericidal effects of**

661 **ciprofloxacin.** **a**, Model fit to experimental time-kill curves. The points indicate the

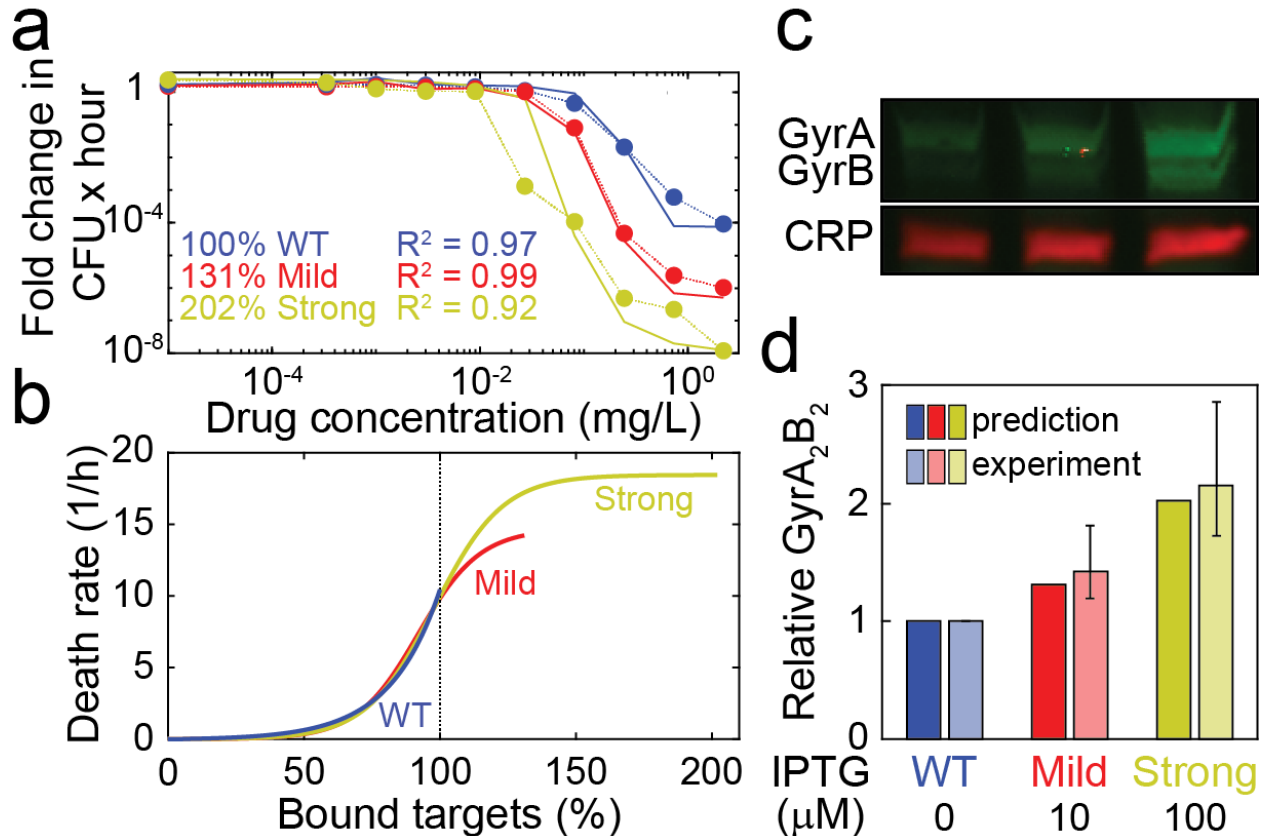
662 experimental data of three independent replicates, and the lines indicate the model fit. Each color

663 indicates a ciprofloxacin concentration as reported in the figure. **b**, The blue line indicates the

664 bacteriostatic effect ($r(x)$, replication rate) of ciprofloxacin and the red line the bactericidal effect

665 ($\delta(x)$, death rate) as a function of the number of bound targets predicted by the model fit in **(a)**.

666 The values of the fitted parameters are listed in Supplementary Tab. S2. **c**, The net growth rate as
667 determined by the slope of a line connecting the initial bacterial density and the final bacterial
668 density of a time-kill curve at 18 h on a logarithmic scale, is given as function of the drug
669 concentration (blue). The dotted horizontal line indicates zero net growth, and the intersection
670 with the blue line predicts the MIC (0.0139 mg/mL).



671

672 **Fig. 4| Prediction of relative antibiotic target molecule content from time-kill curves. a,**

673 Dose-response curves of *E. coli* expressing *gyrA* and *gyrB* under the same IPTG-inducible

674 promoter (SoA3329) grown in the presence of 10 μM IPTG (mild overexpression; red) and 100

675 μM IPTG (strong overexpression; yellow). A control strain (SoA3330), which expresses wild-

676 type GyrAB levels and contains a mock plasmid, is grown in the absence of inducer (blue). The

677 x-axis indicates the ciprofloxacin concentration, and the y-axis indicates the fold change in

678 colony forming units over time. The dotted lines indicate experimental data, and the solid lines

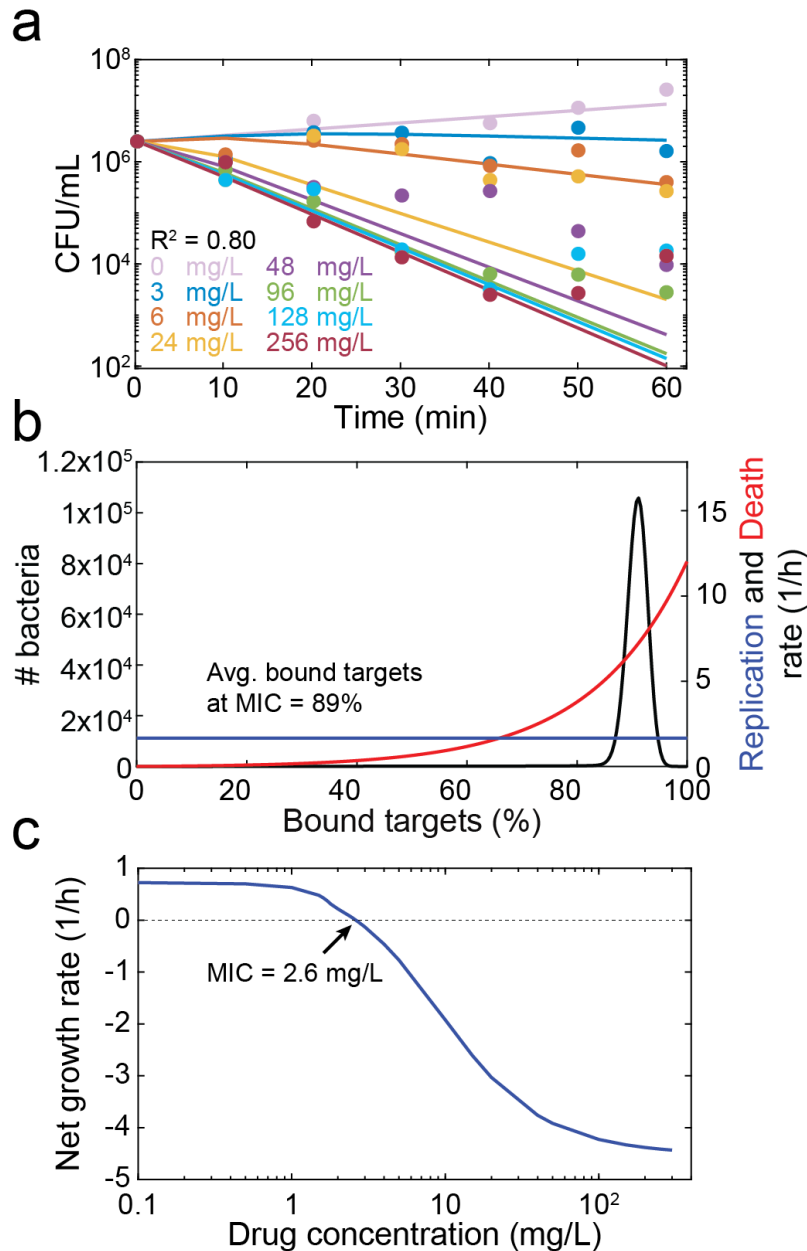
679 indicate the model fit. The best model fit was obtained for relative target molecule contents of

680 131 % (mild overexpression) and 202 % (strong overexpression) relative to the control strain

681 (WT). **b,** Death rates of *E. coli* expressing different levels of GyrAB. The colors represent

682 GyrAB expression conditions as in (a). The x-axis shows the percentage of bound antibiotic

683 target normalized to the control strain; the y-axis shows the death rate $\delta(x)$. Each line represents
684 the best fit for $\delta(x)$. **c**, Western blot analysis of GyrA&B in the strains/conditions shown in **(a)**.
685 CRP (cAMP receptor protein) was used as loading control. A representative example of six
686 replicates is shown; see Supplementary Fig. S2 for full blots. **d**, comparison of theoretical
687 prediction (from **(b)**, solid colors) and GyrA₂B₂ tetramer levels estimated from relative GyrA&B
688 monomer levels (quantified in **(c)**, translucent colors). For the experimental measurements, the
689 bars indicate the mean, and the whiskers represent the 95 % confidence interval.



690

691 **Fig. 5| Model prediction of MIC and target occupancy at MIC for ampicillin. a,** Model fit to

692 previously published time-kill curves³¹. The points represent experimental data, and the lines

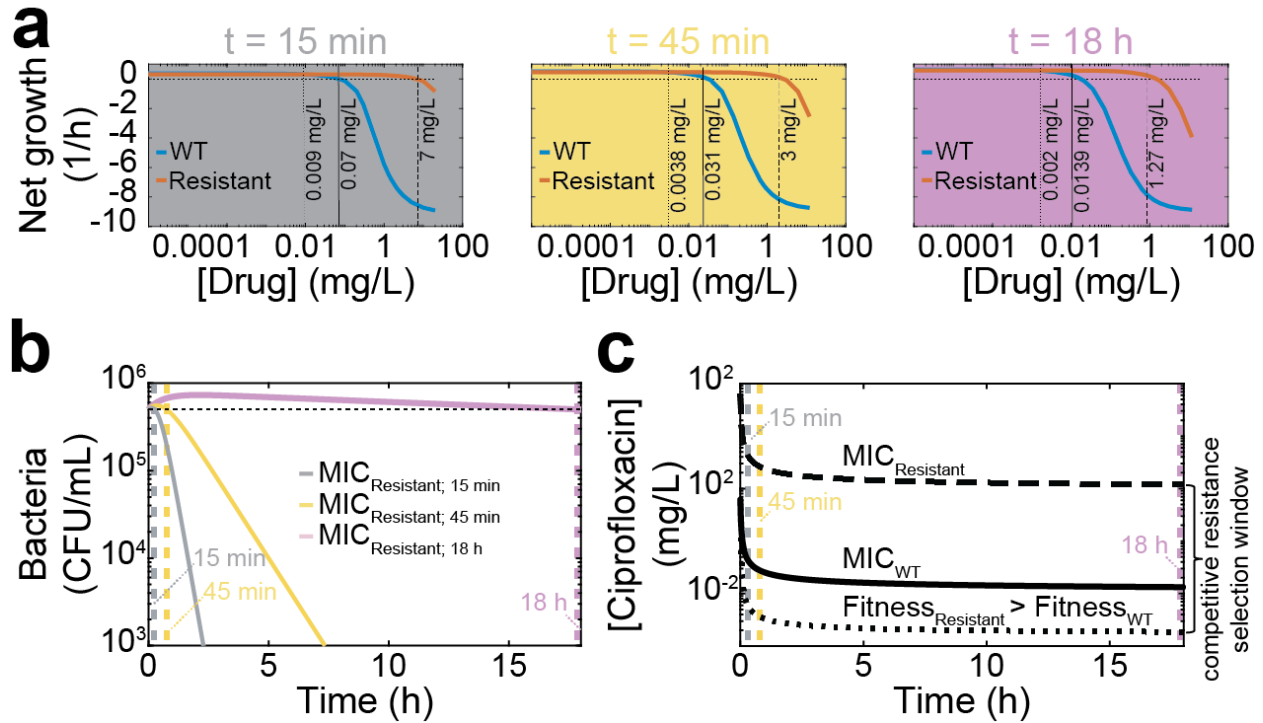
693 represent the fit of the model. Each color indicates a single ampicillin concentration, as described

694 in the legend. **b,** Replication (blue) and death (red) rates as a function of the number of bound

695 targets predicted by the model fit in (a). The black line indicates the predicted distribution of

696 target occupancies in a bacterial population (both living and dead cells) exposed to ampicillin at

697 the MIC for 18 h. **c**, The net growth rate, as determined by the slope of a line connecting the
698 initial bacterial density and the bacterial density at 18 h on a logarithmic scale predicted from the
699 model fit in **(a)**, is shown as function of the drug concentration (blue). The dotted horizontal line
700 indicates zero net growth, and the intersection with the blue line predicts the MIC (2.6 mg/mL).



701

702 **Fig. 6| Predicted mutation selection windows for *E. coli* exposed to ciprofloxacin. a**, The

703 drug concentration of ciprofloxacin is shown on the x-axes, and the average bacterial net growth

704 rate in the first 15 min (grey panel), 45 min (yellow panel), and 18 h (purple panel) of exposure

705 is given on the y-axes. The blue line represents the wild-type strain based on the fits shown in

706 Fig. 3, and the red line represents a strain with a hypothetical resistance mutation that decreases

707 the binding rate (k_f) 100-fold and imparts a 15 % fitness cost. The horizontal dotted line indicates

708 no net growth. The vertical dotted line indicates where the resistant strain becomes more fit than

709 the wild-type, the solid vertical line indicates the MIC of the wild-type, and the dashed vertical

710 line indicates the MIC of the resistant strain. **b**, Modeled time kill curves of the resistant strain

711 for ciprofloxacin concentrations at which there is no growth at 15 min (grey; MIC_{15 min} = 7

712 mg/L), 45 min (yellow; MIC_{45 min} = 3 mg/L) and 18 h (purple; MIC_{18 h} = 1.27 mg/L). The

713 horizontal dotted line indicates the initial population size; the vertical dotted lines represent the

714 time points at which the initial and final population size is the same. **c**, The mutation selection

715 window depends on the time at which bacterial growth is observed. The x-axis shows the
716 observed time at which replication rates were determined, the y-axis shows ciprofloxacin
717 concentrations. The dotted curve shows the ciprofloxacin concentration at which the resistant
718 becomes fitter than the WT ($Fitness_{Resistant} > Fitness_{WT}$), the solid line the MIC of the WT
719 (MIC_{WT}), and the dashed line the MIC of the resistant strain ($MIC_{Resistant}$). The area between the
720 dotted and dashed line indicates the competitive resistance selection window.

721

- 722 1 Boeree, M. J. *et al.* A dose-ranging trial to optimize the dose of rifampin in the treatment of
723 tuberculosis. *Am J Respir Crit Care Med* **191**, 1058-1065, doi:10.1164/rccm.201407-1264OC
724 (2015).
- 725 2 Lan, A. J., Colford, J. M. & Colford, J. M., Jr. The impact of dosing frequency on the efficacy
726 of 10-day penicillin or amoxicillin therapy for streptococcal tonsillopharyngitis: A meta-
727 analysis. *Pediatrics* **105**, E19 (2000).
- 728 3 Roord, J. J., Wolf, B. H., Gossens, M. M. & Kimpen, J. L. Prospective open randomized
729 study comparing efficacies and safeties of a 3-day course of azithromycin and a 10-day
730 course of erythromycin in children with community-acquired acute lower respiratory tract
731 infections. *Antimicrob Agents Chemother* **40**, 2765-2768 (1996).
- 732 4 Van Deun, A., Salim, M. A., Das, A. P., Bastian, I. & Portaels, F. Results of a standardised
733 regimen for multidrug-resistant tuberculosis in Bangladesh. *Int J Tuberc Lung Dis* **8**, 560-567
734 (2004).
- 735 5 WHO. The shorter MDR-TB regimen.
736 http://www.who.int/tb/Short_MDR_regimen_factsheet.pdf?ua=1 (2016).
- 737 6 Waring, M. J. *et al.* An analysis of the attrition of drug candidates from four major
738 pharmaceutical companies. *Nat Rev Drug Discov* **14**, 475-486, doi:10.1038/nrd4609 (2015).
- 739 7 Kouyos, R. D. *et al.* The path of least resistance: aggressive or moderate treatment? *Proc Biol*
740 *Sci* **281**, 20140566, doi:10.1098/rspb.2014.0566 (2014).
- 741 8 Read, A. F., Day, T. & Huijben, S. The evolution of drug resistance and the curious
742 orthodoxy of aggressive chemotherapy. *Proc Natl Acad Sci U S A* **108 Suppl 2**, 10871-10877,
743 doi:10.1073/pnas.1100299108 (2011).
- 744 9 Colijn, C. & Cohen, T. How competition governs whether moderate or aggressive treatment
745 minimizes antibiotic resistance. *Elife* **4**, doi:10.7554/eLife.10559 (2015).
- 746 10 Drlica, K. & Zhao, X. Mutant selection window hypothesis updated. *Clin Infect Dis* **44**, 681-
747 688, doi:10.1086/511642 (2007).
- 748 11 Gullberg, E. *et al.* Selection of resistant bacteria at very low antibiotic concentrations. *PLoS*
749 *Pathog* **7**, e1002158, doi:10.1371/journal.ppat.1002158 (2011).
- 750 12 Drlica, K. The mutant selection window and antimicrobial resistance. *J Antimicrob Chemother*
751 **52**, 11-17, doi:10.1093/jac/dkg269 (2003).
- 752 13 Sommer, M. O. A., Munck, C., Toft-Kehler, R. V. & Andersson, D. I. Prediction of
753 antibiotic resistance: time for a new preclinical paradigm? *Nat Rev Microbiol* **15**, 689-696,
754 doi:10.1038/nrmicro.2017.75 (2017).

- 755 14 Muliaditan, M., Davies, G. R., Simonsson, U. S. H., Gillespie, S. H. & Della Pasqua, O. The
756 implications of model-informed drug discovery and development for tuberculosis. *Drug*
757 *Discov Today* **22**, 481-486, doi:10.1016/j.drudis.2016.09.004 (2017).
- 758 15 Walkup, G. K. *et al.* Translating slow-binding inhibition kinetics into cellular and in vivo
759 effects. *Nat Chem Biol* **11**, 416-423, doi:10.1038/nchembio.1796 (2015).
- 760 16 Sykes, D. A. *et al.* Extrapyramidal side effects of antipsychotics are linked to their association
761 kinetics at dopamine D2 receptors. *Nat Commun* **8**, 763, doi:10.1038/s41467-017-00716-z
762 (2017).
- 763 17 Shen, L. *et al.* A critical subset model provides a conceptual basis for the high antiviral
764 activity of major HIV drugs. *Sci Transl Med* **3**, 91ra63, doi:10.1126/scitranslmed.3002304
765 (2011).
- 766 18 Abel zur Wiesch, P. *et al.* Classic reaction kinetics can explain complex patterns of antibiotic
767 action. *Sci Transl Med* **7**, doi:ARTN 287ra73
768 10.1126/scitranslmed.aaa8760 (2015).
- 769 19 Aldred, K. J., Kerns, R. J. & Osheroff, N. Mechanism of quinolone action and resistance.
770 *Biochemistry* **53**, 1565-1574, doi:10.1021/bi5000564 (2014).
- 771 20 Shen, L. L. & Pernet, A. G. Mechanism of inhibition of DNA gyrase by analogues of
772 nalidixic acid: the target of the drugs is DNA. *Proc Natl Acad Sci U S A* **82**, 307-311 (1985).
- 773 21 Shen, L. L. *et al.* Mechanism of inhibition of DNA gyrase by quinolone antibacterials: a
774 cooperative drug--DNA binding model. *Biochemistry* **28**, 3886-3894 (1989).
- 775 22 Andriole, V. T. <<The>> *quinolones*. 3rd edn, (Academic Press, 2000).
- 776 23 Jungkind, D. L. & American Society for Microbiology Eastern Pennsylvania Branch.
777 *Antimicrobial resistance a crisis in health care*. (Plenum Press, 1995).
- 778 24 Kampranis, S. C. & Maxwell, A. The DNA gyrase-quinolone complex. ATP hydrolysis and
779 the mechanism of DNA cleavage. *J Biol Chem* **273**, 22615-22626 (1998).
- 780 25 Siporin, C., Heifetz, C. L. & Domagala, J. M. *The New generation of quinolones*. (M. Dekker,
781 1990).
- 782 26 Abel Zur Wiesch, P., Clarelli, F. & Cohen, T. Using Chemical Reaction Kinetics to Predict
783 Optimal Antibiotic Treatment Strategies. *PLoS Comput Biol* **13**, e1005321,
784 doi:10.1371/journal.pcbi.1005321 (2017).
- 785 27 Elliott, T. S., Shelton, A. & Greenwood, D. The response of *Escherichia coli* to
786 ciprofloxacin and norfloxacin. *J Med Microbiol* **23**, 83-88, doi:10.1099/00222615-23-1-83
787 (1987).
- 788 28 Silva, F., Lourenco, O., Queiroz, J. A. & Domingues, F. C. Bacteriostatic versus bactericidal
789 activity of ciprofloxacin in *Escherichia coli* assessed by flow cytometry using a novel far-red
790 dye. *J Antibiot (Tokyo)* **64**, 321-325, doi:10.1038/ja.2011.5 (2011).
- 791 29 Garoff, L., Yadav, K. & Hughes, D. Increased expression of Qnr is sufficient to confer
792 clinical resistance to ciprofloxacin in *Escherichia coli*. *J Antimicrob Chemother* **73**, 348-352,
793 doi:10.1093/jac/dkx375 (2018).
- 794 30 Sulavik, M. C. *et al.* Antibiotic susceptibility profiles of *Escherichia coli* strains lacking
795 multidrug efflux pump genes. *Antimicrob Agents Chemother* **45**, 1126-1136,
796 doi:10.1128/AAC.45.4.1126-1136.2001 (2001).
- 797 31 Regoes, R. R. *et al.* Pharmacodynamic functions: a multiparameter approach to the design of
798 antibiotic treatment regimens. *Antimicrob Agents Chemother* **48**, 3670-3676,
799 doi:10.1128/AAC.48.10.3670-3676.2004 (2004).
- 800 32 Palmer, A. C. & Kishony, R. Opposing effects of target overexpression reveal drug
801 mechanisms. *Nat Commun* **5**, 4296, doi:10.1038/ncomms5296 (2014).
- 802 33 Fontana, W. Lecture Notes: Continuous-Time Monte-Carlo of Reaction Systems.

- 803 34 Ocampo, P. S. *et al.* Antagonism between bacteriostatic and bactericidal antibiotics is
804 prevalent. *Antimicrob Agents Chemother* **58**, 4573-4582, doi:10.1128/AAC.02463-14 (2014).
- 805 35 Chambers, H. F., Sachdeva, M. J. & Hackbarth, C. J. Kinetics of penicillin binding to
806 penicillin-binding proteins of *Staphylococcus aureus*. *Biochem J* **301 (Pt 1)**, 139-144 (1994).
- 807 36 Al-Emran, H. M. *et al.* Detection of a Novel *gyrB* Mutation Associated With
808 Fluoroquinolone-Nonsusceptible *Salmonella enterica* serovar Typhimurium Isolated From a
809 Bloodstream Infection in Ghana. *Clin Infect Dis* **62 Suppl 1**, S47-49, doi:10.1093/cid/civ790
810 (2016).
- 811 37 Vogwill, T. & MacLean, R. C. The genetic basis of the fitness costs of antimicrobial
812 resistance: a meta-analysis approach. *Evol Appl* **8**, 284-295, doi:10.1111/eva.12202 (2015).
- 813 38 Jorgensen, J. H. & Ferraro, M. J. Antimicrobial susceptibility testing: a review of general
814 principles and contemporary practices. *Clin Infect Dis* **49**, 1749-1755, doi:10.1086/647952
815 (2009).
- 816 39 Tonge, P. J. Drug-Target Kinetics in Drug Discovery. *ACS Chem Neurosci* **9**, 29-39,
817 doi:10.1021/acschemneuro.7b00185 (2018).
- 818 40 Metcalf, B. J. *et al.* Using whole genome sequencing to identify resistance determinants and
819 predict antimicrobial resistance phenotypes for year 2015 invasive pneumococcal disease
820 isolates recovered in the United States. *Clin Microbiol Infect* **22**, 1002 e1001-1002 e1008,
821 doi:10.1016/j.cmi.2016.08.001 (2016).
- 822 41 Eyre, D. W. *et al.* WGS to predict antibiotic MICs for *Neisseria gonorrhoeae*. *J Antimicrob*
823 *Chemother* **72**, 1937-1947, doi:10.1093/jac/dkx067 (2017).
- 824 42 Payne, D. J., Gwynn, M. N., Holmes, D. J. & Pompliano, D. L. Drugs for bad bugs:
825 confronting the challenges of antibacterial discovery. *Nat Rev Drug Discov* **6**, 29-40,
826 doi:10.1038/nrd2201 (2007).
- 827 43 van der Putten, B. C. *et al.* Quantifying the contribution of four resistance mechanisms to
828 ciprofloxacin minimum inhibitory concentration in *Escherichia coli*: a systematic review.
829 372086, doi:10.1101/372086 %J bioRxiv (2018).
- 830 44 Copeland, R. A. The drug-target residence time model: a 10-year retrospective. *Nat Rev Drug*
831 *Discov* **15**, 87-95, doi:10.1038/nrd.2015.18 (2016).
- 832 45 Srimani, J. K., Huang, S., Lopatkin, A. J. & You, L. Drug detoxification dynamics explain the
833 postantibiotic effect. *Mol Syst Biol* **13**, 948, doi:10.15252/msb.20177723 (2017).
- 834 46 Cramariuc, O. *et al.* Mechanism for translocation of fluoroquinolones across lipid
835 membranes. *Biochim Biophys Acta* **1818**, 2563-2571, doi:10.1016/j.bbamem.2012.05.027
836 (2012).
- 837 47 Hirsch, C. 1 online resource (Butterworth-Heinemann,, Oxford, 2007).
- 838 48 Wu, J. *et al.* The dimer state of *GyrB* is an active form: implications for the initial complex
839 assembly and processive strand passage. *Nucleic Acids Res* **39**, 8488-8502,
840 doi:10.1093/nar/gkr553 (2011).
- 841 49 Maier, T. *et al.* Quantification of mRNA and protein and integration with protein turnover in
842 a bacterium. *Mol Syst Biol* **7**, 511, doi:10.1038/msb.2011.38 (2011).
- 843 50 Malmstrom, J. *et al.* Proteome-wide cellular protein concentrations of the human pathogen
844 *Leptospira interrogans*. *Nature* **460**, 762-765, doi:10.1038/nature08184 (2009).
- 845 51 Datsenko, K. A. & Wanner, B. L. One-step inactivation of chromosomal genes in
846 *Escherichia coli* K-12 using PCR products. *Proc Natl Acad Sci U S A* **97**, 6640-6645,
847 doi:10.1073/pnas.120163297 (2000).
- 848 52 Martinecz, A. & Abel Zur Wiesch, P. Estimating treatment prolongation for persistent
849 infections. *Pathog Dis* **76**, doi:10.1093/femspd/fty065 (2018).

850